RSC Advances

RSC Publishing

COMMUNICATION

View Article Online
View Journal | View Issue

Hybrid gas-phase synthesis of nanoscale Fe–SiO_2 core–shell agglomerates for efficient transfection into cells and use in magnetic cell patterning†

Cite this: *RSC Advances*, 2013, **3**, 13685

Received 1st May 2013,
Accepted 7th June 2013

DOI: 10.1039/c3ra42151a

www.rsc.org/advances

Jeong Hoon Byeon[a] and Young-Woo Kim*[b]

Nanoscale iron (Fe)–silica (SiO_2) core–shell agglomerates were conveniently obtained *via* gas-phase hybridization of freshly produced Fe with SiO_2 synthesized in an aqueous medium containing polyethyleneimine. Synthesized Fe–SiO_2 agglomerates were employed as nanocarriers for gene transfection and magnetic cell patterning *in vitro*.

Iron (Fe), the most ubiquitous of the transition metals, is the structural backbone of our modern infrastructure and among the most useful magnetic materials.[1] Over the past few years, Fe-based nanomaterials have been of great interest for researchers from a wide range of disciplines, including their use in catalysis, data storage, biotechnology/biomedicine, and environmental remediation.[2] In contrast, the high reactivity of Fe has been somewhat unfavorable in biomedical applications, in favor of its own oxides (especially magnetite and maghemite).

Hybrid nanoparticles containing two or more different nanoscale functionalities are attractive candidates for advanced nanomaterials. With controlled structure and interface interactions, these nanoparticles can exhibit novel physical and chemical properties that will be essential for future technological applications.[2] Recently, Fe–Fe_xO_y or Fe–silica (SiO_2) hybrid nanoparticles with high magnetic moment were fabricated for biomedical applications with a much lower magnetic field gradient than has previously been achieved.[3] The SiO_2 layer is also chemically inert over a wide range of pH values, indicating that the core–shell nanoparticles can survive in many solvents. Moreover, the non-toxicity of the SiO_2 layer makes the magnetic nanoparticles highly biocompatible.[4]

Due to their unique magnetic properties, various methods for the preparation of SiO_2 coated metallic nanoparticles have been developed in the last few years. To synthesize these nanoparticles, judicious selection of the reaction conditions is needed to promote heterogeneous nucleation of a target solid onto preformed nanocrystal seeds while avoiding conditions that result in isolated single-component particles. The nanoparticles and their syntheses are becoming increasingly complex, time-consuming, and complicated, and have the potential to form multiple products in the reaction solution,[4] and thus it is still a challenge to prepare the nanoparticles in a simple, green, and continuous synthesis manner.

The regulation of cellular activities (*e.g.* cell signalling) in a controlled manner is one of the most challenging issues in fields ranging from cell biology to biomedicine. Magnetic techniques are uniquely advantageous because magnetic fields can penetrate deeply with negligible attenuation into biological tissues. Consequently, it has distinctive benefits even for *in vivo* applications. When coupled with magnetic nanoparticles, magnetic fields can be transformed into other forms of energy, such as heat and mechanical force.[5] Indeed, an external field aided assembly of living cells within *in vitro* systems is aimed at understanding cellular processes for cell monitoring, selective manipulation, toxicity evaluation, and drug screening.[6]

The present work introduces a continuous hybrid gas-phase synthesis of nanoscale Fe–SiO_2 core–shell agglomerates for their efficient transfection into cells and use in magnetic cell patterning. Fe chain-like nanoparticles were freshly produced in the gas-phase,[7] and the particle-laden flow was passed over an atomizer orifice where they mixed with the atomized SiO_2, ultrasound-assisted synthesized,[8] and were coated by polyethyleneimine (PEI) to form hybrid droplets. The droplets then passed through a heated tubular reactor to drive solvent from the droplets, resulting in nanoscale Fe–SiO_2 core–shell agglomerates (Fig. S1, ESI†). Finally, the Fe–SiO_2 agglomerates were first employed as nanocarriers to facilitate the transfection of protein into cells, and were further used as magnetic carriers to assemble cell arrays.

To prepare fresh Fe nanoparticles in the gas-phase first a spark discharge under a nitrogen environment was employed. The gas temperature inside the spark channel was increased beyond the critical value, which was sufficient to sublimate parts of the Fe electrodes.[7] The duration of each spark was very short ($\sim$1 ms) and the vapors cooled rapidly downstream of the spark. This formed a supersaturation resulting in particle formation through nucleation-condensation. The total number concentration (TNC),

[a]*Department of Chemistry, Purdue University, Indiana 47907, United States*
[b]*Department of Automotive Engineering, Hoseo University, Asan 336-795, Republic of Korea. E-mail: ywkim@hoseo.edu; Fax: +82 41 540 5818; Tel: +82 41 540 5819*

† Electronic supplementary information (ESI) available. See DOI: 10.1039/c3ra42151a

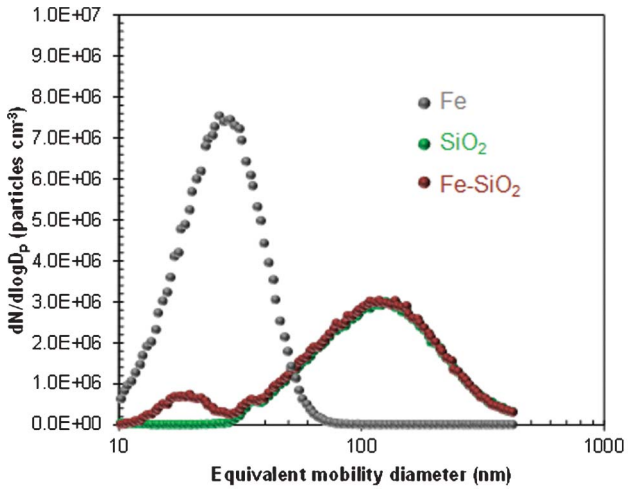

Fig. 1 Size distributions of spark produced Fe, collision atomized SiO_2, and their incorporated structure (Fe–SiO_2) from a hybrid gas-phase route.

geometric mean diameter (GMD), and geometric standard deviation (GSD) of the Fe particles, which were measured using a scanning mobility particle sizer (3936, TSI, US), were 3.18×10^6 particles cm^{-3}, 25.7 nm, 1.46, respectively, as shown in Fig. 1. Fe–SiO_2 hybrid particles were formed by incorporating Fe with SiO_2 during the collision atomization of the SiO_2 solution. We verified incorporation between the Fe and SiO_2 by measuring the size distributions of the SiO_2 and Fe–SiO_2 in the gas-phase. Table S1, ESI† summarizes the size distribution measurements of the SiO_2 and Fe–SiO_2 particles. The GMD, GSD, and TNC of the Fe–SiO_2 particles were 2.12×10^6 particles cm^{-3}, 96.7 nm and 2.09, respectively. The analogous data for individual SiO_2 particles were 1.88×10^6 cm^{-3}, 113.5 nm, and 1.77, respectively. The Fe–SiO_2 case shows a different size distribution compared to the individual Fe and SiO_2 cases, and the Fe peak significantly decreased, implying that the Fe component was nearly quantitatively capsulated by SiO_2 particles, to form Fe–SiO_2 hybrid structures.

Low and high magnification transmission electron microscope (TEM, Libra 120, Carl Zeiss, Germany) images show the morphology of the Fe, SiO_2, and Fe–SiO_2. Specimens were prepared for examination in the TEM by direct electrostatic gas-phase sampling at a sampling flow of 1.0 L min^{-1} and an operating voltage of 5 kV using a Nano Particle Collector (NPC-10, HCT, Korea). The TEM images (Fig. 2) reveal that the spark produced Fe was comprised of chain-like nanoparticles of several primary particles (each $\sim$3 nm in diameter), and as shown in the inset of the Fe image, about 0.202 nm of the lattice fringe was observed, which could be indexed as the (110) plane of the body centered cubic (bcc) Fe crystals. The morphology of the atomized SiO_2 is that of a spherical agglomerate with a size of about 110 nm in mode diameter, which consisted of $\sim$20 nm sized individual SiO_2 spheres. When the chain-like Fe nanoparticles passed over the orifice of the atomizer, it was clear that there were no Fe nanoparticles on the SiO_2 spheres, which confirms that the Fe particles were covered by SiO_2 spheres. One of insets of the Fe–SiO_2 image from a bright field TEM observation proves the presence of Fe chain-like nanoparticles (dark dots in the dotted area) in the SiO_2 matrix. The Fe particles were redistributed to another chain-like structure in the SiO_2 matrix due to de-agglomeration (by setting the force acting on an agglomerate of size D_{pa} due to the sudden pressure change across an orifice in the atomizer), and the size is given by[9]

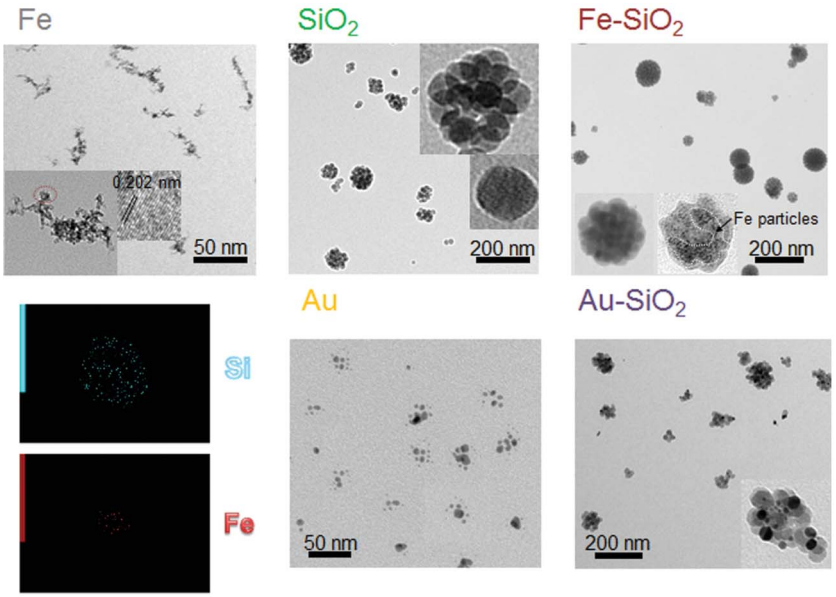

Fig. 2 TEM images of spark produced Fe, collision atomized SiO_2, and their incorporated ''core–shell'' agglomerate structure (Fe–SiO_2) from a hybrid gas-phase route. EDX maps to identify compositions of Fe and Si in the core–shell agglomerates are also displayed. TEM images of spark produced Au and their incorporated structure with SiO_2 (Au–SiO_2) show a different morphology.

$$D_{pr} = \alpha\sqrt{\frac{D_{pa}H}{6\pi\Delta P\Theta^2}} \quad (1)$$

where D_{pr} is the size of a restructured agglomerate, α is the proportionality constant, H is the Hamaker constant, ΔP is the pressure difference between the front and the rear of the orifice, and Θ is the parameter controlling the maximum cohesive strength between the constituting particles. The Fe nanoparticles pass through the orifice, and the rapid changes in pressure, density, and velocity across the orifice produce an impulse capable of restructuring the nanoparticles. The following two images show the energy dispersive X-ray (EDX, JED-2300, JEOL, Japan) maps of the inset image of Fe–SiO_2 agglomerates. These maps correspond to Si and Fe, respectively. The dots in these images indicate the existence of each element in the agglomerate, and thus it could be suggested that the Fe nanoparticles were covered by SiO_2 spheres. Images of Au nanoparticles and their incorporated structures with SiO_2 spheres (Au–SiO_2) under the same operating conditions are also displayed in Fig. 2. The images show the de-agglomerated Au particles with the attached Au particles being smaller and more narrowly dispersed than were the individual Au particles. The mechanism of incorporation between the Fe chain-like nanoparticles and SiO_2 nanoscale spheres in the gas-phase is shown in Scheme 1. The SiO_2 spheres in a hybrid droplet gather on restructured (due to a pressure change between before and after the orifice) Fe particles in the form of Fe–SiO_2 core–shell agglomerates. This phenomenon is different from the incorporation between Au and SiO_2, as shown in the inset of Scheme 1. As seen in the images of the Fe and Au particles (Fig. 2), the different cohesive strengths (Θ) (from the different agglomerate structures) between the particles could induce different incorporation behaviors. As defined in eqn (2),[10] the collision frequency function (K) between Fe (or Au) and SiO_2 could be affected by the size (D_{pr}) of a restructured Fe (or Au) agglomerate. The collision frequency function is given by

$$K = \frac{2kTD_{pp,SiO_2}}{3\mu D_{pr,Fe(or\ Au)}} \quad (2)$$

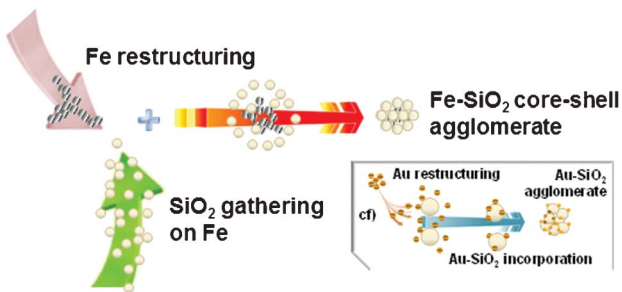

Scheme 1 Mechanism of incorporation between Fe chain-like nanoparticles and SiO_2 nanoscale spheres in the gas-phase. The SiO_2 spheres in a hybrid droplet gather on restructured Fe chain particles in the form of nanoscale Fe–SiO_2 core–shell agglomerates. This phenomenon is different from the incorporation between Au and SiO_2 under the same operation conditions. The de-agglomerated Au particles are deposited on SiO_2 spheres *via* heterogeneous collision between them.

where k is the Boltzmann factor, T is the temperature, and μ is the gas viscosity. More highly de-agglomerated (*i.e.* smaller D_{pr}) Au particles induced a greater heterogeneous collision between the Au and SiO_2, and thus the final morphology could be differentiated between Fe–SiO_2 and Au–SiO_2. The passivation of chain-like Fe nanoparticles by SiO_2 spheres is consistent with a previous report for collisions between Fe and polymer particles.[9]

The crystallinity of the Fe–SiO_2 agglomerates was characterized by X-ray diffraction (XRD, RINT-2100, Rigaku, Japan). Fig. S2a, ESI† shows the XRD patterns of the SiO_2 and Fe–SiO_2 samples. The broad band was centered at about 22° for individual SiO_2 spheres and arises from amorphous SiO_2. For the Fe–SiO_2 sample, there are other diffraction bands at 44.7° and 65.0°, which are assigned to bcc-Fe (110) and (200) planes (JCPDS 06-0696), clearly indicating the nature of heterodimer structures of the Fe and SiO_2. Fourier transform infrared (FTIR, IFS 66/S, Bruker Optics, Germany) spectroscopy was further used to identify the incorporation between the Fe and SiO_2 components during the synthesis (Fig. S2b, ESI†). The FTIR spectrum of Fe–SiO_2 agglomerates shows the characteristic signals at 3500–3200 cm^{-1} (N–H stretching), 2962 cm^{-1} (asymmetric stretching of CH_2), 2847 cm^{-1} (symmetric stretching of CH_2), 1610 cm^{-1} (primary amine) and 1560 cm^{-1} (secondary amine). Another broad band in the low energy region of the spectrum due to the characteristic vibrations of Si–O–Si is observed in the range of 960–1280 cm^{-1}.[11] A peak around at 970 cm^{-1} might also suggest the presence of Si–O–Fe bonds, indicating the presence of surface oxidation on the Fe particles.

As an important character of the Fe–SiO_2 agglomerates, the magnetic properties of the Fe and Fe–SiO_2 samples were characterized using a Lake Shore Cryotronics 7404 vibrating sample magnetometer at room temperature (300 K). These data were presented in electromagnetic units per gram of solid sample. As indicated in Fig. S3, ESI,† at room temperature, both Fe and Fe–SiO_2 samples are consistent with the paramagnetic behavior of Fe, however, the saturation magnetizations of the Fe–SiO_2 show a lower intensity, revealing the diamagnetic contribution from the SiO_2, yet the value from Fe–SiO_2 is still large enough for magnetic separation applications probably due to the unique core–shell agglomerate structure (*i.e.* due to it being magnetically permeable).

We tested the cytotoxicity and gene transfection efficiency of the Fe–SiO_2 agglomerates as a potential material for biomedical applications. The results (Fig. 3a) show that the cell viability was $>\sim$88% for the Fe–SiO_2 agglomerates at different concentrations of 20, 50, 100, 200, and 400 μg mL^{-1}, while the measured viabilities of individual Fe and SiO_2 samples were $>\sim$80% and $>\sim$92%, respectively. It is observed that all the samples exhibited a higher toxicity at a high particle concentration, but there are no significant differences between the SiO_2 and Fe–SiO_2 samples probably due to the passivation by the SiO_2 spheres. This implies that the Fe–SiO_2 has a biocompatibility that may be suitable in a clinical context. The transfection efficiencies of PEI-pDNA complexes in the HeLa cell lines are higher than that from naked DNA (Fig. 3b). Out of these, the efficiency for the synthesized Fe–SiO_2 is the highest, and even higher than that from lipofectamine (Life Technologies, US). Fig. S4, ESI† shows fluorescence images of the cells for the complexes derived from green fluorescent protein

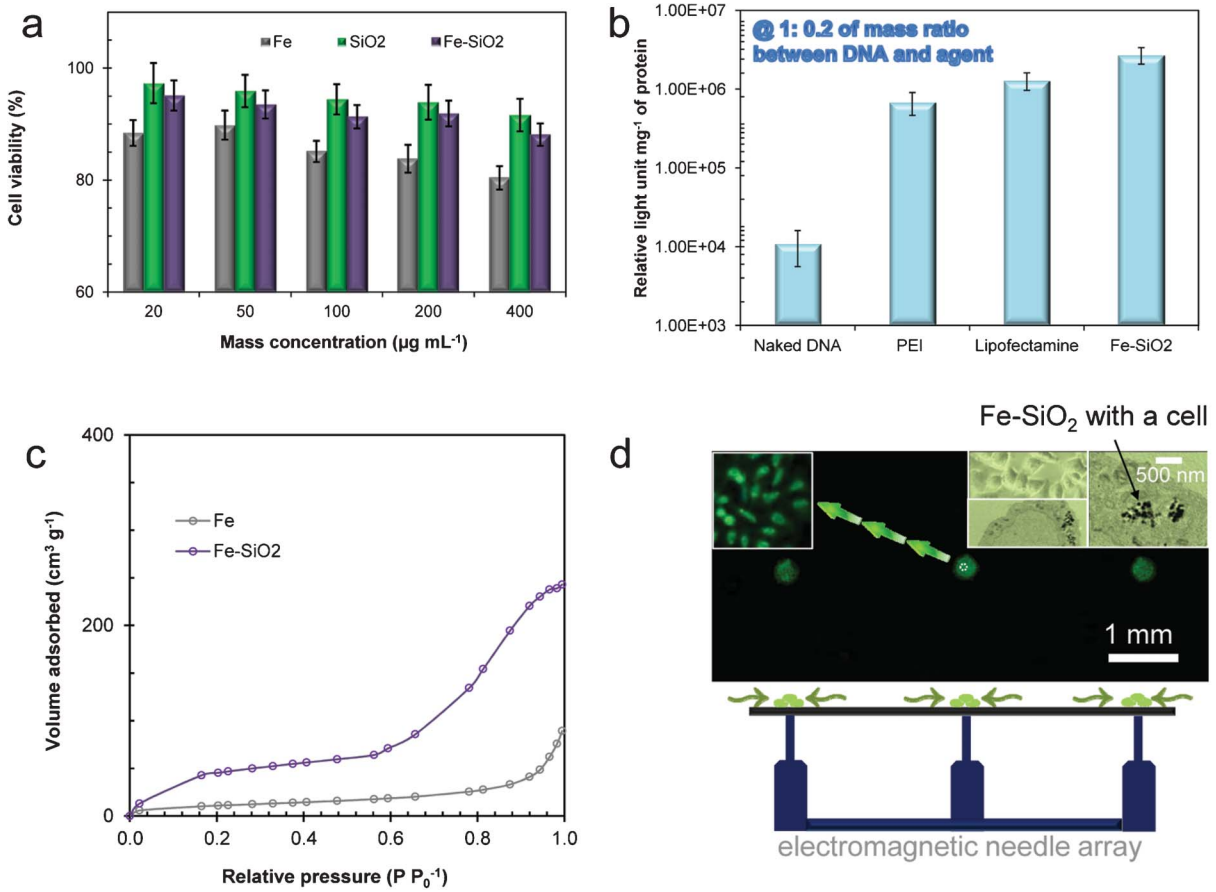

Fig. 3 *In vitro* measurements of (a) cell viability and (b) gene transfection efficiency for spark produced Fe, collision atomized SiO_2, and their incorporated ''core–shell'' agglomerate structure (Fe–SiO_2). (c) Adsorption isotherms of the Fe and Fe–SiO_2 samples. (d) Magnetically assembled dot arrays of Fe–SiO_2-transfected cells.

(GFP) expression, which further confirmed the transfection and differences between the complexes. Fig. 3c shows the nitrogen adsorption isotherms of Fe and Fe–SiO_2 samples. The Fe–SiO_2 exhibits a remarkable increase in the relative pressure range of 0.6–0.9, indicating a narrow mesopore size distribution. The sharp inflections in the isotherms between 0.65 and 0.75 correspond to capillary condensation within uniform mesopores. The Fe nanoparticles show an increase at around 0.8 indicating that the pore size is relatively larger than the Fe–SiO_2 particles. The enhanced surface structure of the Fe–SiO_2 to carry genes might induce a better performance in gene transfection. The number [*i.e.* surface area (S), $S \propto n$] of consisting particles per unit volume (eqn (3))[12] generally increases with decreasing size of the consisting particles, implying that the different transfection efficiencies may be controlled by differentiating the size of consisting particles.

$$n = \frac{0.7405}{\frac{4}{3}\pi\left(\frac{D_c + 2D_g}{2}\right)^3 10^{-21}} \quad (3)$$

where D_c and D_g are the diameter of consisting particles and the gap distance between the consisting particles, respectively. Fig. 3d shows the site-selective assembly of HeLa cells expressing GFP on three identical electromagnetic needles by flowing the cells with buffer solution, which also confirms the GFP transfection. Several dots (inset of Fig. 3d) over the cell indicate the Fe–SiO_2 presence. The microscope image (inset of Fig. 3d) shows larger sizes of the Fe–SiO_2 agglomerates owing to gathering individual agglomerate during their transfection into cells. These dots appear to be inside the cell, implying that PEI incorporation could achieve intracellular transfection. The cell assembly onto the needles in the desired pattern (dot arrays) was achieved, as shown in Fig. 3d, which proves the magnetoactive property of the Fe–SiO_2 in the cells. This non-contact strategy could produce microscale cell patterns without the special preparation of cell solution for contact printing methods. In addition, these agglomerates may also be effective in rapid and highly efficient gene delivery when magnetic force directs the agglomerates towards target cells.[13]

Conclusions

The work presented herein demonstrates that, through hybrid gas-phase synthesis, nanoscale Fe–SiO_2 core–shell agglomerates with cationic components can be made biocompatible and suitable for linking efficient gene transfection and magnetic cell assembly without the use of tedious wet chemical processes. Spark

discharge produced Fe chain-like nanoparticles (~26 nm in equivalent mobility diameter) were quantitatively capsulated by atomized SiO_2 sphere agglomerates (~114 nm) in the form of nanoscale Fe–SiO_2 core–shell agglomerates (~97 nm). Measurements of cell viability and gene transfection efficiency revealed that even though the core–shell agglomerates had a slightly higher cytotoxicity (> ~88% in cell viability) than that of the individual SiO_2 particles (> ~92%), the transfection (2.72×10^6 in RLU per mg of protein) of the genes was enhanced by their porous structure and was even higher than that of lipofectamine (1.28×10^6), a commercial transfection agent. Furthermore, when the magnetic dot field was applied to the aqueous media containing the Fe–SiO_2-transfected cells, the cells were assembled as dot arrays. Although at an early stage of development, the proposed method opens up a new way to obtain both biocompatible and magnetoactive nanomaterials in a sustainable and generalizable manner for a broad range of biomedical applications.

Notes and references

1 D. L. Huber, *Small*, 2005, **1**, 482.
2 (*a*) L. L. Ma, M. D. Feldman, J. M. Tam, A. S. Paranjape, K. K. Cheruku, T. A. Larson, J. O. Tam, D. R. Ingram, V. Paramita, J. W. Villard, J. T. Jenkins, T. Wang, G. D. Clarke, R. Asmis, K. Sokolov, B. Chandrasekar, T. E. Milner and K. P. Johnston, *ACS Nano*, 2009, **3**, 2686; (*b*) C. Wang, C. Xu, H. Zeng and S. Sun, *Adv. Mater.*, 2009, **21**, 3045.
3 (*a*) M.-M. Song, W.-J. Song, H. Bi, J. Wang, W.-L. Wu, J. Sun and M. Yu, *Biomaterials*, 2010, **31**, 1509; (*b*) W. Shim, M. J. Paik, D.-T. Nguyen, J.-K. Lee, Y. Lee, J.-H. Kim, E.-H. Shin, J. S. Kang, H.-S. Jung, S. Choi, S. Park, J. S. Shim and G. Lee, *ACS Nano*, 2012, **6**, 7665.
4 (*a*) M. Li, X. Chen, J. Guan, X. Wang, J. Wang, C. T. Williams and C. A. Liang, *J. Mater. Chem.*, 2012, **22**, 609; (*b*) M. A. Malvindi, V. Brunetti, G. Vecchio, A. Galeone, R. Cingolani and P. P. Pompa, *Nanoscale*, 2012, **4**, 486.
5 M. H. Cho, E. J. Lee, M. Son, J.-H. Lee, D. Yoo, J.-w. Kim, S. W. Park, J.-S. Shin and J. Cheon, *Nat. Mater.*, 2012, **11**, 1038.
6 Y. Cheng, X. Luo, C.-Y. Tsao, H.-C. Wu, J. Betz, G. F. Payne, W. E. Bentley and G. W. Rubloff, *Lab Chip*, 2011, **11**, 2316.
7 (*a*) J. H. Byeon and J. T. Roberts, *ACS Appl. Mater. Interfaces*, 2012, **4**, 2693; (*b*) J. H. Byeon and J.-W. Kim, *Appl. Phys. Lett.*, 2012, **101**, 023117.
8 J. H. Byeon and Y.-W. Kim, *Ultrason. Sonochem.*, 2012, **19**, 209.
9 J. H. Byeon and Y.-W. Kim, *RSC Adv.*, 2013, **3**, 7259.
10 J. H. Byeon and J.-W. Kim, *Atmos. Environ.*, 2012, **54**, 272.
11 E. Thirumal, D. Prabhu, K. Chattopadhyay and V. Ravichandran, *J. Alloys Compd.*, 2010, **502**, 169.
12 M. Drygas and J. F. Janik, *Mater. Chem. Phys.*, 2012, **133**, 932.
13 C. Plank, O. Zelphati and O. Mykhaylyk, *Adv. Drug Delivery Rev.*, 2011, **63**, 1300.